Applying FLD Damage Criteria to Predict Damage Evolution in Polymer Sheets Under Nonlinear Forming Conditions

REZA SHAMIM
School of Aeronautics,
Northwestern Polytechnical University,
Xi'an, Shaan'xi 710072,
CHINA

ORCiD: https://orcid.org/0000-0002-4553-4968

Abstract: - Aerospace parts and other thin-walled constructions with intricate patterns frequently employ sheet polymers. Formability is a crucial consideration since these materials may show damage and fractures during the forming process. Predicting failure modes and comprehending formation limitations are paramount to process design engineers. To forecast damage progression in single-sheet polymer forming processes that are characterized by intricate and nonlinear strain patterns, this work uses a fully integrated elastic-plastic damage model. For components with complex strain trajectories, the model accurately predicts deformation and damage behavior, drawing on theories of finite strain and plane stress plastic deformation. When complicated and nonlinear strain circumstances are present in sheet polymer forming procedures, the combination of finite element analysis with continuum damage mechanics provides a quick and precise way to predict the damage progression.

Key-Words: - Damage evolution, Forming limit diagram, Forming process, Nonlinear deformation, Polymer, Simulation.

Received: April 23, 2024. Revised: October 27, 2024. Accepted: November 14, 2024. Published: December 31, 2024.

1 Introduction

One of the biggest challenges in material forming processes is the prediction and analysis of rupture. It is currently unclear how to accurately estimate when a macrocrack will begin. Defect prediction can now be completed faster than before, mostly due to numerical software. Continuum damage mechanics, which is a local approach to failure, is one of the potential solutions this problem might be solved with [1], [2], [3]. One measure of the material's effective internal degradation after it has been subjected to a local loading is called the damage variable in a represented volume element (RVE). Fracture in an RVE is defined after the last stage of damage progression is identified by a local criterion, [4], [5]. There were some voids and fissures in the materials' microstructure. Most of the time, small flaws grew when the loads reached a particular point. Damage is the build-up of micro stresses around faults or interfaces, which causes bonds to break at the microscale level. The formation and aggregation of microcracks or microvoids that collectively start a single crack at the mesoscale level is damage. At last, this represents the crack's expansion on a macroscale. Studying the development of faults and how they affect a material's mechanical strength is the primary objective of damage mechanics, [6]. We should take into account the elastic-plastic and damage models in the constitutive equations since significant plastic deformation is accompanied by internal deterioration of bonds (damage). In this study, Lemaitre's model for ductile damage progression is integrated with the isotropic elastic-plastic material model. The derived constitutive equations are then applied to predict the initiation and development of fractures during sheet polymer forming processes. The application of the Forming Limit Diagram (FLD) damage criteria to predict damage evolution in polymer sheets under nonlinear forming conditions is a complex task that necessitates a thorough understanding of damage mechanics and material behavior. The FLD is traditionally used to assess the formability of sheet metals, but its application to polymers, particularly under nonlinear conditions, requires careful consideration of the unique damage mechanisms that occur in these materials, [7], [8], [9], [10]. Damage evolution in materials, including polymers, typically follows a sequence of stages: nucleation, growth, and coalescence of microvoids. The Gurson-Tvergaard-Needleman (GTN) damage model is particularly effective in describing these processes, as it accounts for the void volume fraction, which is critical in predicting mechanical properties and potential defects such as rupture and wrinkling during forming processes, [11], [12]. The GTN model has been successfully applied to various materials, including high-strength steels and polymers, demonstrating its versatility in predicting damage under different loading conditions, [13], [14]. In the context of polymer composites, the temperature and damage-dependent tensile strength play a significant role in their formability. The TDDTS model, which incorporates the effects of temperature and damage, highlights the importance of understanding how these factors influence the mechanical behavior of fiber/polymer composites, [15], [16]. This is particularly relevant when considering the nonlinear forming conditions that can lead to complex damage patterns not captured by traditional FLD approaches. Moreover, continuous damage mechanics provides a robust framework for modeling the degradation of polymers. This approach allows for the transformation of geometric discontinuities into the evolution of macroscopic mechanical properties, which is essential for accurately predicting damage under nonlinear conditions, [17], [18]. The integration of Continuum Damage Mechanics with the GTN model can enhance the predictive capabilities for damage evolution in polymer sheets, especially when subjected to varying strain paths and loading conditions. The limitations of conventional FLD models in estimating direct fracture and deformation histories under nonlinear strain paths have been noted in recent studies. For instance, the need for improvements in necking-based failure criteria has been emphasized, as these models often fail to account for the complex interactions that occur in advanced materials like polymers, [19], [20]. The hybrid damage prediction procedure, utilizing a stiffness degradation model and an energy approach, accurately predicts the damage of composite laminates under spectra loading, showing excellent agreement with experimental results, [21].

The incorporation of anisotropic damage models, such as those modified to account for material-induced anisotropic damage, can further refine predictions of formability and damage evolution in polymer sheets, [22], [23]. These findings contribute to human construction and modern environmental Science by enhancing the durability and resilience of polymer-based components used in sustainable infrastructure and eco-friendly transportation solutions, ultimately reducing material waste and improving lifecycle performance in environmentally sensitive applications.

2 Ductile Damage Model

To begin, the principles of Continuum Damage Mechanics are examined in the context of uniaxial stress. In this scenario, isotropic damage is considered to be uniformly distributed across the Representative Volume Element (RVE), [24]. The RVE's cross-sectional area is represented by A, with the assumption that damage within the RVE consists of both voids and cracks. The total area occupied by these defects is denoted as A_D, which leads to an effective cross-sectional area for the RVE, labeled as $\tilde{A}$:

$$\tilde{A} = A - A_D \tag{1}$$

The definition of the damage variable D is then introduced as:

$$D = \frac{A_D}{A} = \frac{A - \tilde{A}}{A} \tag{2}$$

First proposed by Kachanov, is the damage variable. D is defined as 0 in an undamaged state and 1 at full failure. Consequently, the expression is given as:

$$0 \le D \le 1 \tag{3}$$

The RVE, in both its damaged and effective undamaged configurations, is subjected to the same tensile force F. As a result, the effective uniaxial stress can be determined using the following expression:

$$\tilde{\sigma} = \frac{A}{\tilde{A}} \sigma \tag{4}$$

where σ is the true stress in the RVE. By substituting the eq. 2 to eq. 4, the following equation for the effective uniaxial stress is achieved:
σ represents the true stress within the RVE. By substituting equation (2) into equation (4), the expression for the effective uniaxial stress is obtained as follows:

$$\tilde{\sigma} = \frac{\sigma}{1 - D} \tag{5}$$

In the context of irreversible thermodynamics, the energy damage criterion is derived from the damaged elasticity potential, which is part of the state potential and kinetic law. Additionally, damage evolution is determined from the dissipation potential. Assuming small strains and displacements during the thermodynamic process, damage is treated as a state variable, [25], [26]. Consequently, the Helmholtz free energy, ψ, is regarded as a scalar function of these state variables.

$$\psi = \psi\left(\varepsilon_e, \varepsilon_p, T, r, \alpha, D\right) \tag{6}$$

Here, ε_e, and ε_p denote the elastic and plastic strain tensors related to the stress tensor, while T represents the temperature connected to entropy density. The variable r signifies the damage-accumulated plastic strain associated with isotropic strain hardening, and α is the back strain tensor linked to kinematic hardening. A^c is related to the defects of the sample. Assuming the density ρ which serves as an approximation for ductile damage, remains constant, and applying the second law of thermodynamics through the Clausius-Duhem inequality, the relevant variables for an isothermal process can be derived as follows:

$$\begin{gathered} F = \bar{\sigma}^{\upsilon}\left(\bar{A} + A^c\right) \\ F = \bar{\sigma}\bar{A} \\ \bar{\sigma} = \bar{\sigma}^{v}\left(1 + \frac{A^c}{\bar{A}}\right) \end{gathered} \tag{7}$$

In the case of yielding considering the equivalent strain statement the F function will be represented as (8) equations, where R_v is the strain-hardening variable, and X_D is the back stress tensor.

$$F = \left|\frac{\sigma}{1-D} - X_D\right| - R_v - \sigma_y = 0 \tag{8}$$

$$\sigma = \left(\sigma_y + R_v + X_D\right)\left(1-D\right) \tag{9}$$

Here, ε_{pD} is referred to as the strain energy release rate resulting from the stiffness reduction in the RVE where damage has occurred. This variable is also the key factor driving the damage phenomenon.

$$\begin{gathered} \varepsilon_p < \varepsilon_{pD} \rightarrow D = 0 \\ D = D_c \end{gathered} \tag{10}$$

ε_T^+ and ε_T^- are the equivalent plastic strains at the onset of soft damage for the same biaxial tension and compression tests. For isotropic materials, the three-axis stress ratio is the same in the two-axis tension state and the same in the two-axis compression state. ε_T^+, ε_T^- and k_0 are a function of the strain rate material.

$$\varepsilon_{eq}^{**}(\eta) = \frac{\varepsilon_T^+ \sinh\left[k_0\left(\eta^- - \eta\right)\right] + \varepsilon_T^- \sinh\left[k_0\left(\eta - \eta^+\right)\right]}{\sinh\left[k_0\left(\eta^- - \eta^+\right)\right]} \tag{11}$$

In this expression, E denotes the Young's modulus, and σ_{eq} represents the Von Mises equivalent stress. R_v is a function of the triaxiality ratio and in this context, υ represents Poisson's ratio and $\eta = \frac{\sigma_H}{\sigma_{eq}}$ is the triaxiality ratio, where σ_H denotes the hydrostatic stress. Based on Lemaitre's damage criterion, the damage evolution equations in terms of internal variables are:

$$D = \int_0^{\varepsilon_{eq}^{**}} \frac{d\varepsilon_{eq}}{\varepsilon_{eq}^{**}(\eta)} = 1 \tag{12}$$

D is a damage variable that increases uniformly with plastic deformation and is calculated in the following way during the analysis of its positive changes at each stage.

$$\Delta D = \frac{\Delta\varepsilon_{eq}}{\varepsilon_{eq}^{**}} \geq 0 \tag{13}$$

The change initiation criterion continues until the following condition is satisfied.

$$D = \frac{\varepsilon_{major}^A}{\varepsilon_{major}^B} = 1 \tag{14}$$

$$\dot{D} = \frac{\sigma^2}{2rE\left(1-D\right)^2}\dot{\varepsilon}^p \tag{15}$$

Here, $\dot{\varepsilon}^p$ refers to the plastic consistency parameter, while r is the material-specific damage parameter.

3 Numerical Simulations

To solve nonlinear problems, as a rule, numerical methods are used, which include the finite element method. Currently, FEM is the most popular way to solve practical problems of the mechanics of a deformable solid, [27]. With its help, calculations are carried out to determine the stress-strain state and the bearing capacity of real structures of various industries and construction. In this case, problems of both general and local strength are effectively solved. The development of the finite element method for dynamic and nonlinear problems provides the ability to reliably model complex processes such as fracture, impact, loss of stability, stamping, drawing, etc. [28], [29], [30], [31], [32]. Almost all the problems of the solid-state solid-propellant rocket engine were formulated and solved in the framework of finite element techniques. To highlight the core features of Lemaitre's damage model, a numerical example is presented involving a rectangular deep drawing process. This simulation is critical for validating the model due to its complex strain paths, [33], [34], [35]. The verification was carried out using an explicit finite element code, simulating the complex mechanics of the deep drawing process. In this process, a rectangular blank undergoes significant plastic deformation to produce a three-dimensional rectangular box shape. This setup involves a deformable sheet, a rigid punch that drives the forming process, a die that shapes the material, and a blank holder that controls the material flow. The simulation models these components in 3D, capturing the interactions and stresses across each element during deformation. To optimize computational efficiency, the analysis considers only one-quarter of the geometry, leveraging symmetric boundary conditions. This symmetry reduces computational load while retaining full accuracy in the deformation behavior. The die, characterized by a flat surface, features a central rectangular opening measuring 120 mm by 190 mm, with rounded corners (radius of 45 mm) to minimize stress concentration and rounded edges (radius of 20 mm) to facilitate smoother material flow. The rigid punch, square in shape and dimensioned at 100 mm by 150 mm, mirrors the rounding features of the die, ensuring a uniform pressing force during the deep drawing operation. The blank holder, also modeled as a rigid component, is a flat surface that restricts the sheet's movement and applies controlled force along the blank's edges, limiting material flow to avoid wrinkling and ensuring an even draw-in toward the die cavity. Initially, the deformable blank is a flat rectangular sheet with a thickness of 3 mm, which undergoes deformation under the punch's force, forming the desired box shape within the specified die cavity. The detailed schematic of this setup is illustrated in Figure 1.

The blank interacts with the punch, die, and blank holder, all modeled using a 10-node quadratic tetrahedron (C3D10) element in Abaqus. This element is ideal for accurately simulating complex deformations in solid structures, utilizing quadratic interpolation functions to capture intricate shapes and linear deformations in structural analyses. The distance between the blank holder and the die surface is fixed at 0.5 mm. Friction coefficients are 0.18 for the interaction between the punch and the blank and 0.10 for the die-holder and the blank. ABS is the material properties applied for the blank, and its damage characterizations are specified in Table 1.

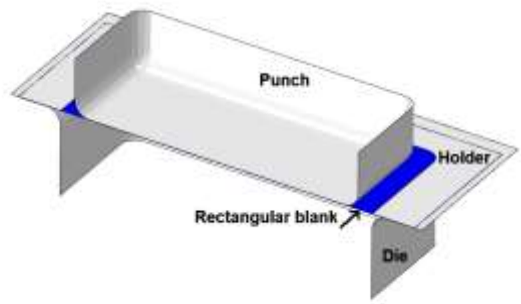

Fig. 1: The schematic of the problem

Table 1. Mechanical properties of ABS Plus

Ultimate strength (MPa)	33
Yield strength (MPa)	31
Elongation at yield (%)	2
Modulus of elasticity (GPa)	2.2
Poisson's ratio	0.36
Density (kg/m^3)	1020
Damage parameter, s	1
Damage parameter, r (MPa)	2.532
Critical damage parameter, D_{cr}	0.434

A subroutine called user material (UMAT) was created as a Fortran program to characterize the material's crystal plasticity behavior. ABAQUS, a non-linear finite element program, was connected to this function. Considering the material's initial texture and its progression over time, our approach allowed us to model an arbitrary plastic deformation. To satisfy the damage initiation requirement, the following conditions must be met: the material must experience sufficient levels of stress and strain that exceed defined thresholds, accounting for factors such as stress triaxiality and strain rate. These parameters collectively indicate when the material's capacity to withstand further deformation without fracturing has been surpassed, triggering the onset of damage.

$$\Delta\omega_D = \frac{\Delta\bar{\varepsilon}^{pl}}{\bar{\varepsilon}_D^{pl}\left(\eta, \dot{\bar{\varepsilon}}^{pl}\right)} \geq 0 \tag{16}$$

Collecting the FLD damage initiation criterion, the ductile criterion is applied to predict the onset of localized necking and eventual fracture in the polymer sheet during the deep drawing process, capturing the material's capacity to undergo plastic deformation before failure.

$$\omega_{FLD} = \frac{\varepsilon_{major}}{\varepsilon_{major}^{FLD}\left(\varepsilon_{minor,}\ f_i\right)} \tag{17}$$

In the forming limit diagram, the condition $\omega_{FLD} = 1$ provides the damage initiation criterion. The variable ω_{FLD} is a function of the current deformation state and is defined as the ratio of the major limit strain on the forming limit diagram evaluated at the current values of the minor principal strain, ε_{minor}, and predefined field variables, f_i, to the current major principal strain, ε_{major}.

The below term provides the equivalent plastic strain at damage initiation as a tabular function between minor and major strains, optionally the equivalent plastic strain rate, and predefined field variables for the definition of the considered damage initiation criterion.

$$\varepsilon_{major}\left(\varepsilon_{minor,}\dot{\bar{\varepsilon}}^{pl}, f_i\right) \tag{18}$$

In the numerical simulation, the ratio of primary strain rates is denoted by α. The software program involved calculates the value of t across a specified time increment, from t to Δt, for each abrupt change in the deformation path.

$$\alpha_t + \Delta t = (1-\omega)\alpha_t + \omega\frac{\Delta\varepsilon_{minor}}{\Delta\varepsilon_{major}} \tag{19}$$

The constitutive equations of rate-dependent crystal plasticity for the slip magnitudes on 12 slip systems are solved in this subroutine. Semi-implicit time integration was used in the following way to achieve this:

$$d\gamma^{\alpha} = \frac{dt}{2}\left[\gamma^{\cdot\alpha}{}_{t} + \gamma^{\cdot\alpha}{}_{t+dt}\right] \tag{20}$$

4 Results

The following images display the full simulations of the deep drawing process for the drawing ratios indicated above together with the blank's damage distribution.

When the depth is 110 mm, the maximum damage seen in Figure 2 is 0.998. This indicates that the material is approaching its critical failure point. As the depth increases, the localized stress concentration intensifies, leading to progressive material degradation. Beyond this depth, even slight increases in loading could result in complete failure or fracture, as the damage variable nears its upper threshold. This observation highlights the importance of considering material behavior at critical depths in order to prevent catastrophic failure under such conditions. The following images display the full simulations of the deep drawing process for the drawing ratios indicated above together with the blank's damage distribution.

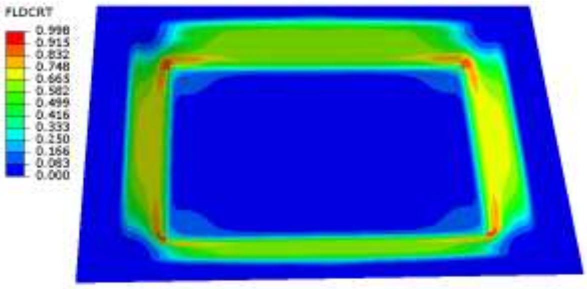

Fig. 2: Initial observation of damage occurrence in the part under loading conditions

Figure 3 demonstrates that the point at which the punch's corner produces a significant amount of plastic deformation is where the rupture starts. It shows the damage that occurred on the surface of the designed model under an applied load of 69 kN and a punch displacement of 115 mm. At this loading condition, surface fractures and localized material failure are evident, particularly in regions with high-stress concentrations. The image clearly illustrates the spread of damage across the surface, with notable deformation near the contact points between the punch and the model. These results suggest that, as the displacement increases, the material experiences significant strain, further contributing to the onset of cracks and potential failure zones within the structure.

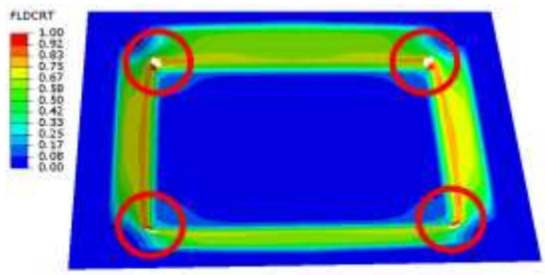

Fig. 3: Identification of the specific damage location within the part

In the vicinity of the blank's edge, wrinkling and damage were also produced when the blank holder force was uncontrolled. Figure 4 shows how the material extends unevenly by illustrating the connection between major and minor strain during deformation. This diagram aids in locating stress channels and forecasts failure modes in the structure, such as necking and localized thinning.

The components of the ductile criterion function as a measure of damage initiation, incorporating the effects of stress triaxiality and strain rate to assess the material's capacity to endure plastic deformation before fracture where the equivalent plastic strain rate is involved.

$$\bar{\varepsilon}_D^{pl}\left(\eta, \dot{\bar{\varepsilon}}^{pl}\right) \tag{21}$$

where η represents the stress triaxiality, defined as the ratio of pressure stress to Mises equivalent stress.

$$\eta = -p / q \tag{22}$$

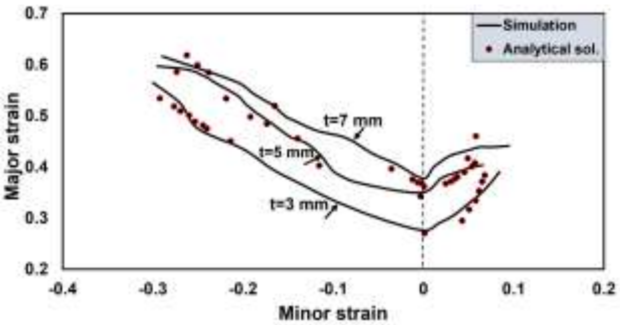

Fig. 4: Relationship between major strain and minor strain during deformation

Figure 5 depicts the equivalent plastic strain path for each critical element of the blank in the forming process, highlighting the elastic and nonlinearity and the plastic strain progression over the sample.

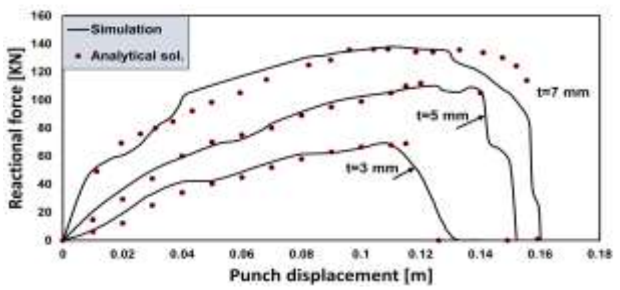

Fig. 5: Force-displacement curve illustrating the mechanical response of the part under loading

Figure 4 and Figure 5 demonstrate a noticeable discrepancy between the numerical simulations and analytical solution results at the peak points for the three examples (3, 5, and 7 mm), with percentage differences of 0.79%, -1.58%, and 1.22%, respectively.

Figure 6 displays two views of damage distribution within the model. On the left, the damage distribution at a depth of 123.5 mm is shown, illustrating how damage progresses within the material at this specific depth. The right side of the figure presents the damage distribution at the end of the process, with a final depth of 135 mm. This comparison reveals the evolution of damage as the process advances, highlighting the increase in damage intensity and its spread throughout the material. The visual contrast between the two depths provides insight into the depth-dependent behavior of damage and its impact on the material's integrity throughout the process.

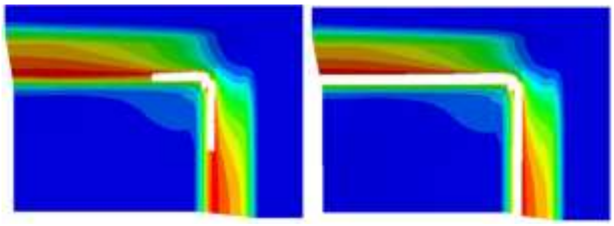

Fig. 6: Left: Damage distribution in depth of 123.5 mm. Right: Damage distribution at the end of process 135mm

5 Conclusion

This study integrates a fully connected elastic-plastic-damage model with an explicit finite element method, employing plane stress and finite strain calculations to simulate the rectangular deep drawing process. The analysis shows that the blank holder's positioning effectively prevents wrinkling, ensuring material integrity. At a depth of 110 mm, maximum damage reached 0.998, indicating a near-critical failure state, where minor loading increases could lead to severe failures. Quantitative data revealed that, under a punch load of 69 kN and a displacement of 115 mm, surface fractures occurred in high-stress regions, highlighting the model's reliability in predicting damage initiation and progression. Figures illustrate damage evolution, showing localized damage at 123.5 mm compared to a more widespread distribution at 135 mm, underscoring the importance of depth-dependent damage behavior. The model's predictive accuracy is vital for optimizing forming processes in the aerospace and automotive industries, enabling engineers to adjust strain limits and deformation paths to reduce fracture risks and extend the service life of thin-walled polymer components. This research advances damage prediction methodologies, promoting more efficient and sustainable manufacturing practices. Additionally, numerical simulation combined with damage continuum mechanics offers a quick and accurate method for predicting damage evolution, rupture, and forming limit curve ratios in polymer forming processes characterized by nonlinear and complex strain paths. Parameters such as strain limits, deformation paths, material properties, and stress concentrations are essential for predicting the FLD Damage Criteria and understanding damage evolution in polymer sheets. Specifically, strain limits define the threshold for material failure, while deformation paths dictate the material's response to applied loads. The inherent material properties, including elasticity, plasticity, and damage tolerance, influence the behavior of polymer sheets under various loading conditions, and stress concentrations at geometric discontinuities significantly impact damage initiation and progression.

Declaration of Generative AI and AI-assisted Technologies in the Writing Process

During the preparation of this work the author used Grammarly for grammar and spell-checking and ChatGPT to improve readability and refine wording. After using this tool/service, the author reviewed and edited the content as needed and takes full responsibility for the content of the publication.

References:

[1] Lemaitre, J., *A Course on Damage Mechanics*, Springer Verlag, Berlin, 1992.

[2] Krajcinovic, D., Damage mechanics, *Mechanics of materials*, Vol. 8, No. 2-3, 1989, pp. 117-197. DOI: 10.1016/0167-6636(89)90011-2.

[3] Vala, J., On a computational smeared damage approach to the analysis of strength of quasi-brittle materials, *WSEAS Transactions on Applied and Theoretical Mechanics*, Vol. 16, 2021, pp.283-292. https://doi.org/10.37394/232011.2021.16.31.

[4] Irwin, G.R., Wells, AA., A Continuum-Mechanics View of Crack Propagation, *Metallurgical Reviews*, Vol. 10, No.1, 1997, pp. 223-270. DOI: 10.1179/mtlr.1965.10.1.223.

[5] Kachanov, L., Introduction to continuum damage mechanics, *Springer Science & Business Media*, Vol. 10, 2013.

[6] Achineethongkham, K. and Uthaisangsuk, V., Analysis of forming limit behaviour of high strength steels under non-linear strain paths using a micromechanics damage modeling, *International Journal of Mechanical Sciences*, Vol. 183, 2020, pp.105828. DOI: 10.1016/j.ijmecsci.2020.105828.

[7] Basak, S. and Panda, S.K., Use of uncoupled ductile damage models for fracture forming limit prediction during two-stage forming of aluminum sheet material, *Journal of Manufacturing Processes*, Vol. 97, 2023, pp.185-199. DOI: 10.1016/j.jmapro.2023.04.042.

[8] Bharti, S., Gupta, A., Krishnaswamy, H., Panigrahi, S.K., and Lee, M.G., Evaluation of uncoupled ductile damage models for fracture prediction in incremental sheet metal forming, *CIRP Journal of Manufacturing Science and Technology*, Vol. 37, 2022, pp.499-517. DOI: 10.1016/j.cirpj.2022.02.023.

[9] Zhang, M., Mirza, H.A., Zhang, Y.C., Tabasum, M.N., Lang, H.L. and Zou, P.Z., Investigation into a comprehensive forming limit curve considering multi-parameters effects for semi-cured FMLs through uniform pressure loading test, *International Journal of Damage Mechanics*, Vol 32, No. 2, 2023, pp.289-317. DOI: 10.1177/10567895221135054.

[10] Tekkaya, A.E., Bouchard, P.O., Bruschi, S. and Tasan, C.C., Damage in metal forming, *CIRP Annals*, Vol. 69, No. 2, 2020, pp.600-623. DOI: 10.1016/j.cirp.2020.05.005.

[11] Berezhnoi, D. V., Shamim, M. R., Numerical investigation of clinch connection manufacturing process, *Procedia Engineering*, Vol. 206, 2017, pp, 1056-1062. DOI: 10.1016/j.proeng.2017.10.594.

[12] Karim, B., Mohand, O. O., Nasereddine, Z., Sébastien, T., Investigation of the influence of incremental sheet forming process parameters using response surface methodology, *Metallurgical Research & Technology*, Vol. 118, No. 4, 2021, pp 401. DOI: 10.1051/metal/2021039.

[13] Yoon, J. S., Noh, H. G., Song, W. J., Kang, B. S., Kim, J., Comparison of experimental and numerical failure criterion for formability prediction of automotive part, *Advanced Materials Research*, No. 658, 2013, pp. 354-360. DOI: 10.4028/www.scientific.net/AMR.658.354.

[14] Isavand, S. and Assempour, A., Effects of microstructural morphology on formability, strain localization, and damage of ferrite-pearlite steels: experimental and micromechanical approaches, *Metallurgical and Materials Transactions A*, Vol. 52, 2021,

pp.711-725. DOI: 10.1007/s11661-020-06115-2.

[15] Nasir, M. W., Chalal, H., Abed-Meraim, F., Formability prediction using bifurcation criteria and GTN damage model, *International Journal of Mechanical Sciences*, No. 191, 2021, pp. 106083. DOI: 10.1016/j.ijmecsci.2020.106083.

[16] Li, Y., Li, W., Zhang, X., Shao, J., Deng, Y., Modeling and influencing factor analysis for the temperature and damage dependent tensile strength of fiber/polymer composites, *Polymer Composites*, Vol. 43, No. 8, 2022, pp. 5573-5581. DOI: 10.1002/pc.26869.

[17] Zirakashvili, N., On the numerical solution of some two-dimensional non-classical elasticity problems by boundary element method, *WSEAS Transactions on Applied and Theoretical Mechanics*, Vol. 14, 2019, pp.17-27.

[18] Su, J., Cheng, J., Zhao, G., Hu, X., Tao, J., Degradation simulation of Poly (L-lactic acid) (PLLA) vascular stents based on the continuous damage model, *Journal of Physics: Conference Series*, Vol. 2256, No. 1, 2022. pp. 012027. DOI: 10.1088/1742-6596/2256/1/012027.

[19] Karyakin, M. and Obrezkov, L., Radial Compression Stability of a Nonlinearly Elastic Cylinder with Internal Stresses, *WSEAS Transactions on Applied and Theoretical Mechanics*, Vol. 14, 2019, pp.159-163.

[20] Pereira, R., Peixinho, N., Sérgio L. Costa. S. L., A Review of Sheet Metal Forming Evaluation of Advanced High-Strength Steels (AHSS), *Metals*, Vol. 14, No. 4, 2024, pp 394. DOI: 10.3390/met14040394.

[21] Khavin, G., Zhiwen, H., Predictions of tool wear by estimating weight loss during polymer composites processing, *Design, construction, maintenance*, Vol. 3, 2023, pp. 293–300. DOI: 10.37394/232022.2023.3.29.

[22] Bousfia, M., Aboussaleh, M., Ouhbi, B., Hybrid damage prediction procedure for composite laminates submitted to spectra loading, *WSEAS transactions on applied and theoretical mechanics*, Vol. 15, 2021, pp. 248–257. https://doi.org/10.37394/232011.2020.15.27.

[23] Niazi, M. S., Wisselink, H. H. Meinders, V. T., Van Den Boogaard, A. H., Material-induced anisotropic damage in DP600, *International Journal of damage mechanics*, Vol. 22, No. 7, 2013, pp. 1039-1070. DOI: 10.1177/1056789512468914.

[24] Egorova, O.V. and Hein, T.Z., Improvement of mechanical properties of polymer materials by the nanosized ceramic particles, *WSEAS Transactions on Applied and Theoretical Mechanics*, Vol. 16, 2021, pp.134-141. https://doi.org/10.37394/232011.2021.16.14.

[25] Öchsner, A., *Continuum damage mechanics*, Springer Singapore, 2016.

[26] Rynkovskaya, M., Alexandrov, S. and Elberdov, T., Plane Strain Expansion of a Cylindrical Cavity in an Infinite Porous Rigid/Plastic Medium Obeying a General Yield Criterion, *WSEAS Transactions on Applied and Theoretical Mechanics*, Vol. 18, 2023, pp.318-326. https://doi.org/10.37394/232011.2023.18.30.

[27] Shamim, R., Exploring the impact on contact adhesion layer properties in numerical simulations, *PLoS ONE*, Vol. 19, No.10, 2024. DOI: 10.1371/journal.pone.0312436.

[28] Guo, Y.M. and Moriki, K., The Elastic-Plastic Micromechanical Response of the Particle Volume Fraction and the Average Size of Particles, *WSEAS Transactions on Applied and Theoretical Mechanics*, Vol. 14, 2019, pp.82-89.

[29] Shahzamanian, M.M. and Wu, P.D., Study of forming limit diagram (FLD) prediction of anisotropic sheet metals using Gurson model in MK method, *International Journal of Material Forming*, Vol. 14, 2021, pp.1031-1041. DOI: 10.1007/s12289-021-01619-7.

[30] Vobejda, R., Šebek, F., Kubík, P. and Petruška, J., Solution to problems caused by associated non-quadratic yield functions with respect to the ductile fracture, *International Journal of Plasticity*, Vol. 154, 2022, pp.103301. DOI: 10.1016/j.ijplas.2022.103301.

[31] Lee, H.W. and Basaran, C., A review of damage, void evolution, and fatigue life prediction models, *Metals*, Vol. 11, No. 4, 2021, pp.609. DOI: 10.3390/met11040609.

[32] Shamim, R., Investigation of bending and crush behaviors in polymer lattice structures: Computational approaches and experimental evaluation, *Journal of Reinforced Plastics and Composites*, 2024, pp. 07316844241273043. DOI: 10.1177/07316844241273043.

[33] Fincato, R. and Tsutsumi, S., Coupled elasto-viscoplastic and damage model accounting for plastic anisotropy and damage evolution dependent on loading conditions, *Computer*

Methods in Applied Mechanics and Engineering, Vol. 387, 2021, pp.114165. DOI: 10.1016/j.cma.2021.114165.

[34] Rong, H., Hu, P., Ying, L., Hou, W. and Dai, M., Modeling the anisotropic plasticity and damage of AA7075 alloy in hot forming, *International Journal of Mechanical Sciences*, Vol. 215, 2022, pp.106951. DOI: 10.1016/j.ijmecsci.2021.106951.

[35] Voyiadjis, G. Z., Continuum damage mechanics, Materials Modeling: Methods, *Dordrecht: Springer Netherlands*, 2005, pp. 1183-1192.

Contribution of Individual Authors to the Creation of a Scientific Article (Ghostwriting Policy)

Reza Shamim: Investigation; methodology; data curation; writing original draft; conceptualization; formal analysis, resources.

Sources of Funding for Research Presented in a Scientific Article or Scientific Article Itself

The author received no financial support for the research, authorship, and/or publication of this article.

Conflict of Interest

The authors declare that they have no known competing financial interests or personal relationships that could have appeared to influence the work reported in this paper.

Data availability statement

The data that support the findings of this study are available from the corresponding author upon request.